JOURNAL OF CATALYSIS 143, 492–498 (1993)

Adsorption of CO on Small Supported Rhodium Particles: SSIMS and TPD Study

V. MATOLÍN,[1] K. MAŠEK,[2] M. H. ELYAKHLOUFI, AND E. GILLET

Laboratoire de Microscopie et Diffractions Electroniques, Faculté des Sciences et Techniques de Saint-Jérôme, Université Aix-Marseille III, 13397 Marseille Cedex 20, France

Received December 21, 1992; revised March 22, 1993

The adsorption of carbon monoxide on small rhodium particles prepared by vapour deposition of Rh on either MgO or alumina supports has been investigated by static secondary ion mass spectrometry (SSIMS) and temperature-programmed desorption (TPD). Part of the CO molecularly adsorbed on clean particles undergoes dissociation during heating. The dissociation is more important for smaller particles. The intensity ratios Rh_nC^+/Rh_n^+ and Rh_nO^+/Rh_n^+ measured by SSIMS have been used to monitor the buildup of surface carbon and oxygen. Carbon recombination with oxygen followed by thermal desorption of CO is associated with the occurrence of high-temperature desorption features and with the disappearance of the carbidic and oxidic relative intensity in SSIMS. Evidence has been obtained for subsurface diffusion of oxygen.

1. INTRODUCTION

Metal catalysts used in most industrial processes consist of small metal particles ranging in size from 1 to 50 nm supported on a porous oxide. It has been shown long ago that, for so-called structure-sensitive reactions, the particle size can affect the catalytic activity by virtue of a size-dependent distribution of specific adsorption sites on small metal particles (*1–3*). Rhodium is a widely used noble metal catalyst: one of its most important applications is in automobile catalytic converters, where addition of Rh provides high conversion for both the NO–CO and the $CO–O_2$ reactions (*4*). As a consequence, numerous studies of CO adsorption and these reactions have been performed in the past. Much attention has been paid to model studies with well defined catalyst surfaces (single crystals) under well defined vacuum conditions.

It is generally assumed that on transition metals located to the left side of a borderline drawn across the Periodic Table from Co to W dissociation occurs during CO adsorption, whereas on transition metals to the right of the line CO usually adsorbs in molecular form. Rhodium is close to this boundary and therefore structural effects on the adsorption behaviour may be expected. Theoretical results (*5, 6*) obtained for CO adsorption on rhodium single crystals show that the bonding interaction with the $2\pi^*$ antibonding orbital increases with the coordination number and that dissociative adsorption at steps is favoured. Partial CO dissociation was reported to occur on Rh(755) and Rh(331) (*7*), Rh(110) (*8*), and Rh(210) (*9, 10*). However, the densely packed Rh(111) (*11, 12*) and Rh(100) (*13, 14*) surfaces were never found to be capable of breaking the C–O bond. CO adsorption studies on Rh model catalysts indicate that there is not an important size effect (*3, 15*) which is related to changes in the distribution of exposed crystal planes as the particle size is varied (*3*).

Static secondary ion mass spectrometry (SSIMS) and temperature-programmed desorption (TPD) provide a very powerful

[1] To whom correspondence should be addressed.

[2] Permanent address: Department of Electronics and Vacuum Physics, Charles University, V Holešovičkách 2, 18000 Prague 8, Czech Republic

0021-9517/93 $5.00

combination for CO adsorption studies. Studies on a wide range of single-crystal surfaces over a number of years have demonstrated that SSIMS is able to discern clearly between the dissociative and the molecular states of adsorption of CO; the data can be used to monitor surface coverage of the adsorbate and the actual stoichiometry of the CO layer adsorbed on a metal, M. The coverage and the symmetry of the bonds can thus be monitored using the relative intensities of the M_n^+ and M_nCO^+ cluster ions (*16–18*). It is also possible to correlate the surface coverage of adsorbed CO during the catalytic oxidation by monitoring the sum of ratios M_nCO^+/M_n^+ with the reaction rate $d(CO_2)/dt$. The occurrence of the $M_mC_n^+$ ion clusters in a SSIMS spectrum is indicative of carbon at the surface (*19*).

In the present paper we report on results obtained in an investigation of CO adsorption over small Rh particles deposited on both alumina and MgO.

2. EXPERIMENTAL

The studies reported here were performed in a specially designed UHV system. This system contains two chambers which can be isolated from each other. The main analysis chamber has facilities for SIMS and temperature-programmed experiments. The second preparation chamber was used for sample preparation and for temperature-programmed desorption. The rhodium particles were grown by vapour deposition. The Rh source was a specially designed microelectron bombardment evaporation source, the atomic flux of which was electronically stabilised and calibrated by a quartz microbalance. The usual flux employed for rhodium deposition was 1×10^{13} atoms cm^{-2} s^{-1}. A special sample holder allowed the transfer of the sample between the two chambers and also temperature programmable heating.

For the experiments described here we used both thermally oxidised (24 hours in air at 900 K) aluminium foil and MgO(001) cleavage as supports for metal particle growth. The alumina layer prepared in this way is a continuous crystalline layer composed of approximately 0.1 μm crystals of γ-alumina (*20*). The back side of the oxidized Al foil was lightly scribed by a steel needle and the samples were submerged in 10% NaOH water solution in order to create very small (several μm) windows by dissolution of aluminium. These windows appeared in the places of the holes created by the scribing and were covered by an intact alumina layer on the front side. After the experimental run, disks of 3 mm diameter were cut from the samples and mounted on the electron microscope grid holder (without grid) for transmission electron microscope (TEM) observation. The particles deposited on MgO were removed from the support using the transfer replica method (*21*).

After Rh deposition the samples were pretreated by heating in CO/O_2 mixture for 1 h in order to obtain stabilised particle structure and morphology. The SSIMS studies were performed using a quadrupole mass spectrometer, with range of 1–600 a.m.u. and ion energy filter, and an ion gun with differential pumping. The primary ion source provides a beam of argon ions with energy up to 5 kV and the incident angle on the sample plane is 45°. The experimental conditions were examined in order to optimise signal intensities and to minimise damage caused to the particle surface during the analysis. Thus a low primary ion current density was used (5 nA cm^{-2} at 3 keV), such that the crystallographic and chemical integrity of the surface layer was preserved during the period of study. The conservation of the integrity of the surface layer was verified by the stability of the SSIMS signals. The sample electrostatic charge, due to the polarisation of insulator supports during the ion impact, was neutralised by a low energy electron beam of 200 eV.

By analogy with the approaches established for the adsorption systems CO/Pd and C/Pd (*19, 21, 22*), we make use of the ion intensities Rh_nCO^+, Rh_n^+, Rh_nC^+, and Rh_nO^+ to follow trends in the development

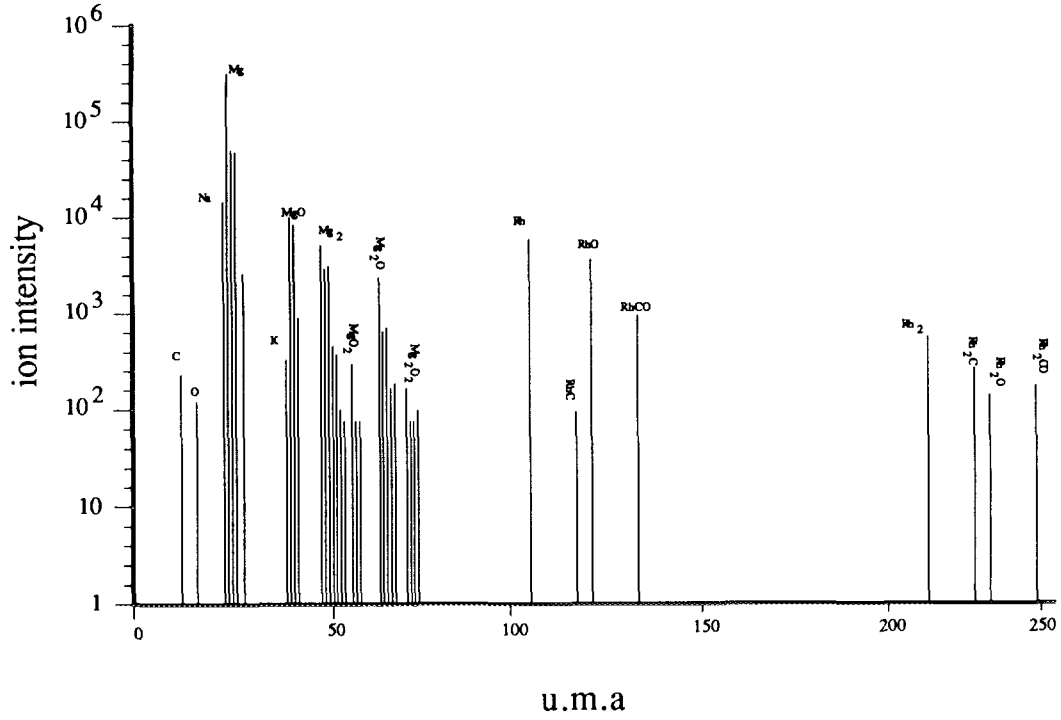

FIG. 1. SSIMS of Rh particles on MgO.

of the surface coverage of the respective species: the sum of ion intensity ratios

$$S_x = \Sigma_n \mathrm{Rh}_n X^+ / \mathrm{Rh}_n^+ \ (n = 1,2;\ X = \mathrm{CO}, \mathrm{C}, \mathrm{O}).$$

shows a direct correlation with the coverage θ_x of X species. A representative SSIMS spectrum of the most important ion intensities obtained for Rh/MgO particles is presented in Fig. 1. The relatively large signals of K^+ and Na^+ are due to the high SIMS sensitivity for these species which are present in the support at very low concentrations.

The TPD profiles were recorded with 5 K/s heating rate using a quadrupole mass spectrometer.

3. RESULTS

3.1. Rhodium Catalyst Morphology

In order to be able to correlate surface properties and particle structure and morphology, we investigated the mechanism of Rh particle growth on different supports. It has been observed that in the case of MgO and alumina the particles grow three-dimensionally. Particle size and structure depend on the properties and the temperature of the support as well as on the deposition rate. It has been shown that under identical conditions the rhodium deposit gives larger particles on the alumina support than on MgO. Similarly the heating under CO/O_2 mixture performed in order to stabilise particle size causes more important coalescence in the case of Rh/alumina. This effect can be explained by longer diffusion lengths of Rh atoms on alumina than on MgO. More details about the results of rhodium growth study will be published in a special paper (*23*).

In order to be able to compare the CO adsorption on particle populations which are very different in size and density, the experiments have been performed on two

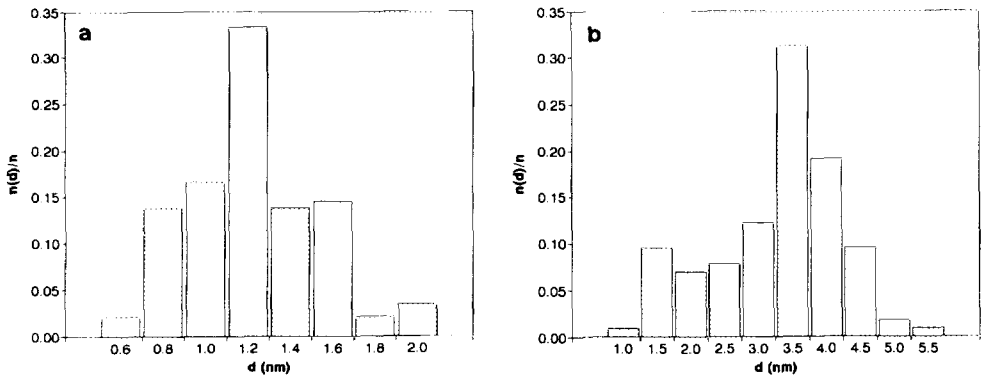

FIG. 2. Size histogram of Rh particles deposited on (a) MgO and (b) alumina; d is the particle diameter, and $n(d)/n$ is the relative number of particles of diameter d.

samples: (A) Rh particles deposited on MgO (001), average particle size ϕ = 1.3 nm and average particle density $d = 1.0 \times 10^{13}$ cm^{-2}; and (B) Rh/Al_2O_3, ϕ = 3.3 nm, $d = 2.9 \times 10^{12}$ cm^{-2}. The size histograms obtained for samples A and B after the whole experimental run are represented in Figs. 2a and 2b. The support (substrate) temperature during deposition was held at 600 K for both samples.

3.2. CO Adsorption

CO adsorption was investigated by combining the TPD and SSIMS methods. All the TPD results were obtained for saturation CO coverage. Figures 3a and 3b represent SSIMS data of one complete adsorption/desorption cycle in comparison with TPD curves. We can see that there is one main molecular binding state, hitherto denoted α, and it exhibits a peak temperature of 440 K. In addition to the α-CO peak a β-peak appears at 520 K. The occurrence of this second peak is interpreted as being due to the recombination of C_{ad} and O_{ad} previously deposited on the surface during activated dissociation of CO, i.e., during the heating procedure. This interpretation is deduced from the SSIMS data: (i) maximum carbon concentration occurs after desorption from the α-state with simultaneous disappearance of CO_{ad} species, and (ii) surface carbon

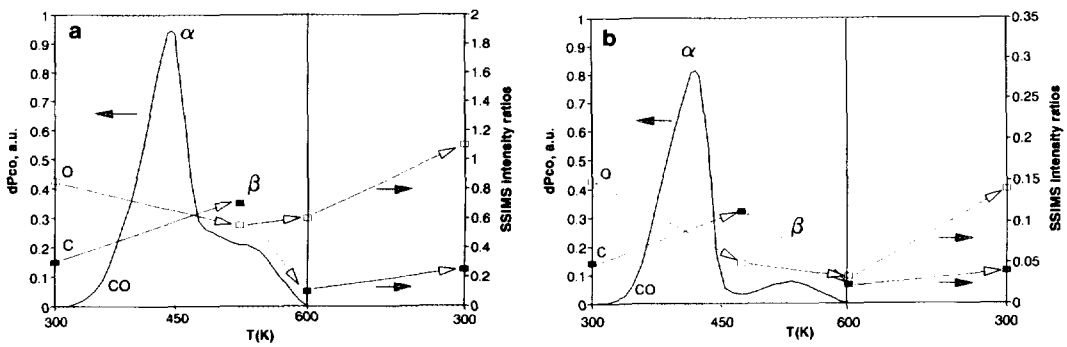

FIG. 3. CO TPD profiles (—) combined with SSIMS $\Sigma_n Rh_n C^+/Rh_n^+$ (■) and $\Sigma_n Rh_n O^+/Rh_n^+$ (□) (n = 1,2) signal ratios measured at different temperatures. After TPD, the samples were cooled to room temperature. (a) 1.3-nm Rh/MgO particles and (b) 3.3-nm Rh/alumina particles.

is removed after desorption of the β-state. This is in agreement with our previous results on Pd (*22*) and with the results obtained on Rh(210) (*9*, *10*). Comparison of the α- and β-peak areas reveals that about 25% and 10% of the adsorbing CO undergoes dissociation on the A and B samples, respectively. The small enhancement of carbon surface concentration observed during sample cooling is probably due to the dissociation of a small amount of CO species readsorbed from the background atmosphere (less than 0.3 L, 1 L = 1.33×10^{-4} Pa s), because it is observed simultaneously with increase of CO_{ad} concentration. It should be noted that after the CO/O_2 treatment and the CO-adsorption/desorption experiments the background atmosphere (about 1×10^{-7} Pa) is composed essentially of CO due to the memory effect of the UHV system. If one considers that the CO/Rh adsorption stoichiometry (CO coverage) at saturation on small supported particles is $\theta_c = 0.9$ (*21*), one can estimate that θ_c after α-state desorption is 0.22 for sample A and 0.09 for sample B. By comparing these values with the SSIMS signal enhancement it is possible to quantify the sum of signal ratios S_c in terms of absolute carbon coverage. Approximate values have been calculated from the above results using the following relationships:

$\theta_c = 0.5\ S_c$ for smaller particles (sample A)
and
$\theta_c = 1.3\ S_c$ for larger ones (sample B).

As can be seen in Figs. 3a and 3b, the variations of oxygen ion intensity ratios, S_o, do not correlate with the carbon ion intensity ratios, S_c, which would be expected from the stoichiometry of CO dissociation. After the desorption of the α-state, oxygen surface concentration decreases while carbon surface concentration increases. This behaviour cannot be simply explained in terms of removing oxygen from the surface by its reaction with CO to CO_2 because in this case there would be a lack of oxygen for its recombination with C to CO during the β-desorption when carbon is completely reacted off.

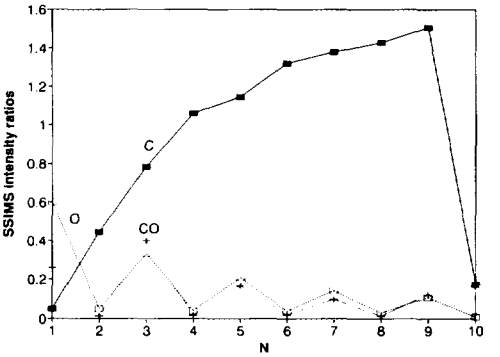

FIG. 4. $\Sigma_n Rh_n C^+/Rh_n^+$ (■), $\Sigma_n Rh_n CO^+/Rh_n^+$ (+), and $\Sigma_n Rh_n O^+/Rh_n^+$ (□) (n = 1,2) intensity ratios as a function of number N of CO adsorption/desorption cycles (only α-state desorptions) for Rh/MgO particles.

In Fig. 4 the difference between C_{ad} and O_{ad} behaviour during CO-adsorption/desorption processes is well seen. The sample A was treated under oxygen in order to remove the surface carbon. We then performed the following series of experiments: adsorption of 1 L of CO, desorption of the α-state only, cooling down to 300 K. Number 1 on the x-axis in Fig. 4 indicates the initial state of the experiment, namely, oxygen and CO adsorption, numbers 2, 4, 6, and 8 correspond to the α-state desorptions and numbers 3, 5, 7, and 9 to the cooling. After the whole series the α- and β-states were completely desorbed, (number 10). It is seen that during the series the carbon surface layer builds up steeply due to the CO_{ad} dissociation whereas the oxygen surface concentration oscillates. The 10th stage represents the situation after total CO desorption (after heating up to 600 K). The carbon layer is depleted by recombination with accumulated oxygen. Afterwards we continued the same experiment but with complete desorptions ($\alpha + \beta$). Only small carbon and oxygen oscillations were observed without accumulation of them (see Fig. 5). Numbers 12, 14, 16, and 18 correspond to the $\alpha + \beta$-state desorption after adsorption of 1 L of CO. Numbers 11, 13, 15, 17, and 19 represent

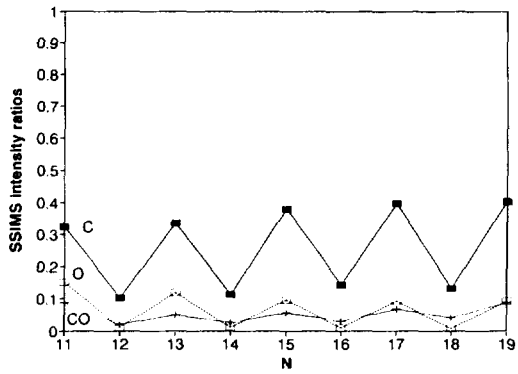

FIG. 5. $\Sigma_n Rh_n C^+/Rh_n^+$ (■), $\Sigma_n Rh_n CO^+/Rh_n^+$ (+), and $\Sigma_n Rh_n O^+/Rh_n^+$ (□) (n = 1,2) intensity ratios as a function of number N of CO adsorption/desorption cycles (only $\alpha+\beta$-state desorption) for Rh/MgO particles.

the state of surface after cooling down to 300 K.

4. DISCUSSION

The occurrence of CO dissociation at metallic surfaces is usually interpreted as concomitant donation of electrons from the CO 5σ orbital into unoccupied metal orbitals and back-donation from metal orbitals into the CO $2\pi^*$ orbital (antibonding system). A large filling of these states upon chemisorption weakens the C–O bond considerably and may even lead to its dissociation. It was shown for Rh that in the case of structural irregularities of a surface on the atomic scale there is a very favourable $2\pi^*$ interaction resulting in higher $2\pi^*$ orbital occupancy (*5*). In the case of small supported particles the number of edge, corner, and step atoms related to the number of plane atoms increases with decreasing particle size. For this reason it seems reasonable to explain the appearance of surface carbon during interaction of the particle surface with CO by dissociation of CO adsorbed near the surface irregularities. We can clearly distinguish between two different CO-desorption features (α and β) where the β-peak results from C_{ad}–O_{ad} recombination. Only desorption of the α-peak produces an enhancement of surface carbon concentration (see Fig. 4). On the other hand, appearance of surface oxygen does not correlate with appearance of surface carbon. Whilst the C_{ad} concentration increases after α-desorption, the increase of O_{ad} concentration is not observed by SSIMS. This shows that there is no oxygen adsorbed in the first atomic layer, which is analysed by SSIMS. Nevertheless, oxygen is present in the sample and it reacts with the surface carbon during heating of the sample to 600 K and removes it completely. The cooling of the particle after α-desorption produces increase of O_{ad} concentration as well as further accumulation of surface carbon. Thus O_{ad} concentration oscillates whilst C_{ad} concentration is builtup steeply. The disappearance of surface oxygen is in agreement with a similar effect observed on Rh(210) (*9*, *10*) which is explained by oxygen surface penetration leading to the occupation of subsurface states. A similar effect has been observed in the case of oxygen on Rh(110) (*24*) where a subsurface state is proposed after heating above 470 K. The appearance of oxygen at the surface during sample cooling can be explained by temperature dependent dissociation of CO which is adsorbed on the surface from the background atmosphere. The asymptotic increase of the "carbon" curve and the decrease in amplitude of oxygen oscillations in Fig. 4 are due to the blocking of adsorption sites by deposited carbon which causes a simultaneous decrease in the dissociative activity of the surface.

It has been shown that the occupation of subsurface states on Rh (*9*, *10*, *24*, *25*) at higher temperatures is accompanied by rhodium surface reconstruction. In the case of very small particles of a diameter corresponding to ten or a lower number of atoms the reconstruction would change considerably the particle structure and morphology. This behaviour could be influenced by oxygen coadsorption with surface carbon as well as by the coadsorption with CO. It is difficult to say more about these effects without the simultaneous investigation of particle structure changes. In order to be

able to give more details about the adsorption-induced phenomena we are performing *in situ* investigations of particle structure and morphology by reflection high energy electron diffraction (RHEED).

5. CONCLUSION

(1) Vacuum vapour deposition of rhodium on MgO and alumina supports induces three-dimensional Rh particle growth with relatively narrow size distribution.

(2) The combined application of SSIMS and TPD has revealed that adsorbed CO partially dissociates during heating to 450 K. An estimated 25 and 10% of CO adsorbed on 1.3 and 3.3 nm Rh particles, respectively, dissociates. Carbon and oxygen recombination to CO leads to the appearance of a β-CO desorption feature at 520 K.

(3) Evidence of subsurface diffusion of oxygen atoms has been obtained. The β-state has been assigned to CO formation and thermal desorption after reversible conversion of the subsurface atoms into surface species.

REFERENCES

1. Goodman, D. W., Kelley, R. D., Madey, T. E., and Yates, J. T., *J. Catal.* **63,** 226 (1980).
2. Kelley, R. D., and Goodman, D. W., *Surf. Sci.* **123,** 743 (1982).
3. Altman, E. I., and Gorte, R. J., *Surf. Sci.* **195,** 392 (1988).
4. Anderson, J. R., and Boudart, M. (Eds.), "Catalysis-Science and Technology," Vol. 5. Springer-Verlag, Berlin/New York, 1984.
5. De Koster, A., Jansen, A. P. J., van Santen, R. A., and Geerlings, J. J. C., *Faraday Discuss. Chem. Soc.* **87,** 263 (1989).
6. De Koster, A., and van Santen, R. A., *Surf. Sci.* **233,** 366 (1990).
7. Castner, D. G., and Somorjai, G. A., *Surf. Sci.* **83,** 60 (1979).
8. Marbrow, R. A., and Lambert, R. M., *Surf. Sci.* **67,** 489 (1977).
9. Rebholtz, M., Prins, R., and Kruse, N., *Surf. Sci.* **259,** L797 (1991).
10. Rebholtz, M., Prins, R., and Kruse, N., *Surf. Sci.* **269/270,** 293 (1992).
11. Yates, J. T., Williams, E. D., and Weinberg, W. H., *Surf. Sci.* **91,** 562 (1980).
12. Castner, D. G., Sexton, B. A., and Somorjai, G. A., *Surf. Sci.* **71,** 363 (1978).
13. Kim, Y., Peebles, H. C., and White, J. M., *Surf. Sci.* **114,** 363 (1982).
14. Gurney, B. A., Richter, L. J., Willarrubia, J. S., and Ho, W., *J. Chem. Phys.* **87,** 6710 (1987).
15. Belton, D. N., and Schmieg, S. T., *Surf. Sci.* **202,** 238 (1988).
16. Brown, A., and Vickerman, J. C., *Surf. Sci.* **151,** 319 (1985).
17. Brown, A., and Vickerman, J. C., *Surf. Sci.* **117,** 154 (1982).
18. Brown, A., and Vickerman, J. C., *Surf. Sci.* **124,** 267 (1983).
19. Matolin, V., and Gillet, E., *Surf. Sci.* **238,** 75 (1990).
20. Ricci, M., Thesis, Université Aix-Marseille III, 1991.
21. Gillet, M. F., and Channakhone, S., *J. Catal.* **97,** 427 (1986).
22. Matolín, V., Rebholtz, M., and Kruse, N., *Surf. Sci.* **245,** 233 (1990).
23. Mašek, K., Matolín, V., and Gillet, M. F., submitted for publication.
24. Bowker, M., Guo, Q., and Joyner, R., *Surf. Sci.* **253,** 33 (1991).
25. Comelli, G., Dhanak, V. R., Kiskinova, M., Pangher, N., Paolucci G., Prince, K. C., and Rosei, R., *Surf. Sci.* **260,** 7 (1992).